International Journal for Housing Science and Its Applications
Publish August 10, 2025. Volume 46, Issue 4 Pages 8216-8228

https://doi.org/10.70517/ijhsa464703

Research on the Optimization of the Load-bearing Capacity of Short Steel-Concrete Columns Using Genetic Algorithms

Qingyun Ge[1,*], Jing Zheng[1], Fulian Yang[1] and Caimei Li[2]
[1] School of Architecture and Civil Engineering, West Anhui University, Lu'an, Anhui, 237012, China
[2] Gates Winhere Automobile Water Pump Products (Yantai) Co., LTD., Yantai, Shandong, 712000, China
Corresponding authors: (e-mail: 05000050@wxc.edu.cn).

Abstract This paper conducts a systematic study on the axial compressive strength of short columns in steel-concrete composite structures (CE-CFST), revealing their mechanical properties and failure mechanisms. A refined finite element model was established using ABAQUS to analyze the interaction between the steel tube and concrete interface and the material constitutive relationships. A bearing capacity prediction model based on a BP neural network was proposed, and its interpretability was verified using the SHAP method. The research results show that for specimens with a steel tube thickness of $t = 3mm$, the circumferential tensile prestress of the CE-CFST-3 steel tube is $183\mu\varepsilon$, which is only about 0.17 times the yield strain of the steel tube, with a strength ratio of 1.05. For specimens with a steel tube thickness of $t = 5mm$, the bearing capacity also increases significantly. The BP neural network model performed best among the comparison models, with the contribution of each parameter to the results decreasing in order from ρ_x, f_c, t, L, f_y, to ρ_y.

Index Terms CE-CFST, finite element analysis, BP neural network, bearing capacity prediction, SHAP

I. Introduction

With China's rapid economic development, the construction of transportation infrastructure has also developed rapidly. Bridge construction in China has increasingly expanded into remote mountainous and canyon regions, facing challenges such as long spans, great heights, heavy loads, and harsh environmental conditions. This has driven engineers and scholars to continuously innovate, proposing and applying various new structural forms [1]-[3]. Among these, steel-reinforced concrete composite structures (CE-CFST) have been particularly widely adopted [4].

The steel-reinforced concrete composite structure (CE-CFST) is a new high-performance composite structure developed by wrapping reinforced concrete around steel-reinforced concrete components (CFST) [5]. Compared to steel-reinforced concrete structures, CE-CFST structures significantly reduce the amount of steel used in the steel framework, making them both economical and environmentally friendly, thereby contributing to China's "carbon peaking" goals [6], [7]. Additionally, steel tube concrete reinforced frames have features such as modular transportation and overall assembly, making them suitable for harsh construction conditions in mountainous areas. Furthermore, the steel tube segments of steel tube concrete can be lifted using cables, greatly reducing the construction difficulty of large-span arch bridges [8]-[10].

Regarding the load-bearing performance of steel tube concrete reinforced composite columns, previous researchers have conducted various experimental and theoretical analyses under different load conditions and component types. Reference [11] simulated the load-bearing capacity of steel-reinforced concrete slender columns under axial compression loads by considering initial defects in long columns in the model, finding that the strength of steel has a negligible effect on load-bearing capacity, and comparing the simulation results with code requirements. Reference [12] investigated the performance of asymmetrical carbon fiber-reinforced polymer (CFRP) wrapped expansive concrete composite beams, finding that the bending load-bearing capacity of the specimens increases with an increase in the steel ratio. Literature [13] investigated the response of reinforced concrete-filled steel tubes (R-CFST) under different concrete strength conditions and compared their performance with that of concrete-filled steel tubes. The study found that R-CFST outperforms CFST in terms of post-peak response, ductility, strength, and resistance to brittle fracture. Literature [14] used finite element analysis and experimental data to study the flexural performance of CE-CFST structures, finding that thin-walled steel tubes can achieve full plastic strength without local buckling, and proposed a Laza model and simplified formula for predicting flexural capacity. Literature [15] conducted axial compression tests on 8 hollow sandwich square steel tube concrete and 8 hollow sandwich round steel tube concrete specimens, with 3 specimens of each section subjected to long-term loading.

The long-term loading was applied for 1,050 days, during which temperature and humidity were kept constant. In terms of bearing capacity, the specimens subjected to long-term loading were slightly lower than those not subjected to long-term loading, but the difference was insignificant.

In CE-CFST structures, steel tube concrete-reinforced composite columns are primarily used as vertical load-bearing members. The nodes formed by CE-CFST columns and RC beams constitute a new type of composite node configuration, which has been widely applied in actual engineering projects [16]-[18]. Regarding the seismic performance of such nodes, foreign scholars have conducted some pseudo-static tests and finite element studies. Literature [19] investigated the bond performance between steel tubes and recycled concrete. The test results indicated that the bond performance of RAC-FST in steel tube concrete is similar to that of the bond performance on the surface of steel tube concrete. Based on the test results, the study analyzed the effects of chemical bonding force, mechanical interlocking force, and steel tube errors on bond strength and proposed a bond strength calculation formula. Literature [20] analyzed the hysteretic performance of hexagonal steel tube concrete-reinforced composite structures, studied the distribution of internal forces and the development of stress, and ultimately proposed a bearing capacity calculation method applicable to hexagonal steel tube concrete-reinforced composite structures. Literature [21] investigates the interface properties of recycled steel tube concrete, conducting four repeated pull-out tests. The study analyzes the failure modes, slip relationships, and bonding mechanisms of the specimens, with results indicating that bonding strength decreases as the size of the steel tube interface increases. Based on component theory research, some scholars have also conducted system analysis. Literature [22] employs the fiber model method to study the hysteretic performance of steel tube concrete-reinforced hybrid columns-steel-reinforced concrete beam frames and proposes a corresponding hysteretic model for the frame.

Steel-reinforced concrete, due to its internal steel reinforcement, can achieve high bearing capacity and good seismic performance, but it also increases construction duration [23]. Since steel-reinforced concrete emerged earlier, there have been numerous research findings on its performance under monotonic loading and hysteretic loading. Reference [24] studied the shear performance and shear bearing capacity of composite nodes with five different column cross-sectional forms. The test results indicated that the flanges of the cross-sectional form significantly enhance the shear bearing capacity, and components with cross-sectional flanges exhibit a notable improvement in shear bearing capacity. Reference [25] investigated the bearing capacity of cross-shaped concrete-filled steel tube columns under axial and eccentric compression, analyzed various parameters to understand their effects, and developed practical design formulas for maximum bearing capacity. Literature [26] investigated the performance of L-shaped prestressed concrete columns with internal I-shaped steel under axial compression through experiments and numerical simulations. The results indicated that higher steel tube constraint indices and higher proportions of internal steel can enhance the column's strength and ductility. Reference [27] proposed a stirrup-constrained concrete-filled steel tube (CFST) composite beam aimed at improving structural performance by mitigating local instability. The study demonstrated significant improvements in bending stiffness and ultimate load-carrying capacity and developed a performance model for predicting structural engineering applications. Literature [28] conducted a comprehensive study on the compressive performance of circular short steel-concrete composite columns with external confinement and internal reinforcement. The results indicated that the axial load-carrying capacity and stiffness of such columns were significantly enhanced, and specimens with bolts and reinforcement components exhibited extremely high reliability.

In summary, research on CFST is relatively well-developed, while studies on CE-CFST remain limited. Additionally, direct environmental effects can exacerbate interface bond failure between the two materials, adversely affecting their normal load-carrying capacity and durability. Furthermore, there are significant differences between the interfaces of CE-CFST and CFST steel tubes: the former involves concrete constraining the steel tube, while the latter involves the steel tube constraining the core concrete. Therefore, research findings from CFST may not be fully applicable to CE-CFST.

This paper first establishes a CE-CFST finite element model based on ABAQUS, focusing on analyzing the contact behavior at the steel pipe-concrete interface and material constitutive behavior. A bearing capacity calculation method based on equivalent constraint coefficients is proposed, and a short column axial compression bearing capacity prediction model is constructed using a BP neural network. Through multi-industry reliability verification and load-deformation relationship analysis, the structural safety of CE-CFST structures is evaluated. Design control experiments to validate the superior predictive performance of the BP neural network model. Use TreeSHAP for interpretability analysis to explore the parameter sensitivity of CE-CFST.

II. Finite element analysis of the axial bearing capacity of short columns in steel tube concrete composite structures

II. A. Finite element analysis of the interface between steel pipe concrete reinforced composite columns

II. A. 1) Model Establishment

The concrete in the CE-CFST column was simulated using three-dimensional eight-node linear reduced integral solid elements (C3D8R). Reinforcing bars and stirrups were modeled using truss elements, with the load transfer between concrete and reinforcing bars simulated using an embedded approach, without considering slip between reinforcing bars and concrete. There are two simulation methods for steel pipes: one uses four-node reduced integral shell elements (S4R), and the other uses solid elements (C3D8R). This paper established finite element models using both methods for preliminary analysis. The results showed that the outcomes from the two steel pipe simulation methods were similar, and when using shell elements, convergence issues arose. Therefore, this paper adopted solid elements to simulate the steel pipes.

This paper primarily investigates the interface between the outer concrete and steel pipe of the CE-CFST, with the inner CFST functioning as an integral component. Throughout the loading process, no slippage occurs at the interface between the steel pipe and core concrete. Therefore, during simulation, the interface between the steel pipe and core concrete within the inner CFST is simulated using a bounding method. To ensure computational accuracy and efficiency, after multiple preliminary analyses, the mesh sizes for the steel pipe and concrete were determined to be 12 mm and 10 mm, respectively.

II. A. 2) Material constitutive relations

(1) Core Concrete Constitutive Model

In ABAQUS, concrete simulation generally employs a plastic damage model for concrete. This model is based on a continuous linear damage model for isotropic plasticity under tension and compression, used to describe the nonlinear behavior of concrete, effectively simulating the complex loading conditions of real concrete. Using a function expression related to the constraint effect coefficient ξ, the core concrete equivalent stress-strain relationship model makes the plastic damage model in ABAQUS applicable to steel-concrete composite structures. An example of the CDP model is shown in Figure 1. This model is selected for the uniaxial compressive stress-strain relationship of core concrete in this paper.

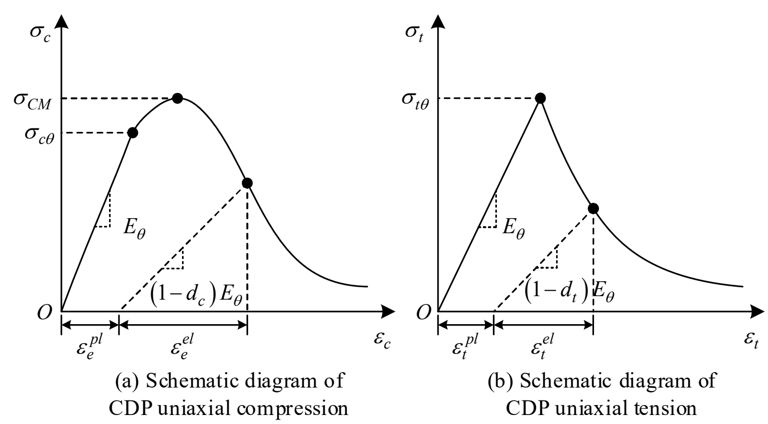

Figure 1: Demonstration of CDP model

$$y=\begin{cases}2x-x^2 & (x\le 1)\\ x/\left[\beta_0(x-1)^2+x\right] & (x>1)\end{cases} \tag{1}$$

$$\xi=\frac{A_s f_y}{A_c f_{ck}} \tag{2}$$

$$\beta=0.6\left(2.44\times10^{-5}\right)^{\left[0.3+(\xi-0.5)^2\right]} f_c^{0.5}\ge 0.15 \tag{3}$$

In the equation, $x=\varepsilon/\varepsilon_0$; $y=\sigma/\sigma_0$; $\sigma_0=f_c$; $\varepsilon_0=\varepsilon_c+750\xi^{0.25}\times10^{-6}$; f_c is the compressive strength of the concrete cylinder; A_s is the cross-sectional area of the steel pipe; A_c is the cross-sectional area of the core concrete; f_y is the yield strength of the steel; f_{ck} is the standard value of the axial compressive strength of the concrete.

The constitutive relationship for uniaxial tensile stress in concrete is as follows:

$$y=\begin{cases}1.4x-0.3x^6 & (x\le 1)\\ x/\left[0.28\sigma_p^2(x-1)^{2.1}+x\right] & (x>1)\end{cases} \tag{4}$$

$$\sigma_p=0.27(1.3f_c)^{2/3} \tag{5}$$

$$\varepsilon_p=50.2\sigma_p\ (\mu\varepsilon) \tag{6}$$

In the equation, σ_p is the peak tensile stress; ε_p is the strain corresponding to the peak tensile stress.

(2) Steel constitutive model

For high-strength steel, a bilinear model is generally selected, which consists of an elastic segment and a strengthening segment. The modulus of the strengthening segment can be taken as 0.01 E_s .

(3) UHPC concrete constitutive model

The constitutive relationship of stirrup-constrained UHPC is shown in Figure 2(a):

Ascending segment

$$f_c=\frac{f_{cc}k\left(\varepsilon_0/\varepsilon_{cc}\right)^k}{k-1+\left(\varepsilon_0/\varepsilon_{cc}\right)^k} \tag{7}$$

$$k=\frac{E_{cc}}{E_{cc}-\left(f_{cc}/\varepsilon_{cc}\right)} \tag{8}$$

downward segment

$$f_c=\exp\left(k_1\left(\varepsilon_0-\varepsilon_{cc}\right)^{k_2}\right)f_{cc} \tag{9}$$

$$k_1=\ln 0.6/\left(\varepsilon_{cs0}-\varepsilon_{cc}\right)^{k_3} \tag{10}$$

$$k_2=0.62+18\left(f_{le}/f_{co}\right)^{1.4} \tag{11}$$

$$f_{le}=0.6k_e f_s\rho_v \tag{12}$$

$$k_e=\frac{\left(1-\sum_{i=1}^{m}\frac{w_i^2}{5b_{cot}^2}\right)\left(1-\frac{s'}{3b_{cot}}\right)^2}{1-\rho_{cc}} \tag{13}$$

In the equation, f_{cc} is the peak compressive strength of the constrained concrete; ε_{cc} is the strain corresponding to f_{cc}; E_{cc} is the secant modulus of confined concrete; s' is the net spacing of stirrups; s is the center-to-center spacing of stirrups; w is the width of stirrups; b_{cot} is the area of confined concrete by stirrups; ρ_{cc} is the reinforcement ratio, and ρ_v is the volume reinforcement ratio.

The tensile constitutive relationship curve is shown in Figure 2(b), and the relationship is as follows:

$$I\ \sigma(\varepsilon)=f_{ct}\varepsilon/\varepsilon_{ca}\quad 0\le\varepsilon\le\varepsilon_{ca} \tag{14}$$

$$II\ \sigma(\varepsilon)=f_{ct}\quad \varepsilon_{ca}\le\varepsilon\le\varepsilon_{cp} \tag{15}$$

$$III\ \sigma(w)=f_{ct}/\left(1+w/w_p\right)^p\quad 0<w \tag{16}$$

In the equation, f_{ct} is the cracking stress of UHPC; ε_{ca} is the cracking strain of UHPC; ε_{cp} is the ultimate tensile strain of UHPC; w is the crack width.

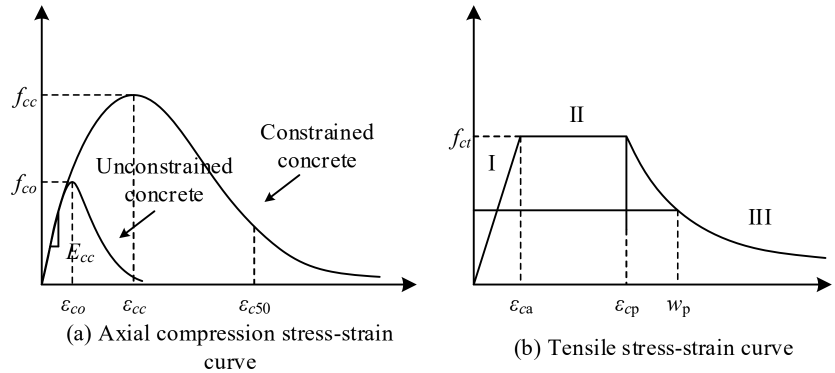

Figure 2: The constitutive relation of UHPC

II. B.Finite element analysis of the axial bearing capacity of steel tube concrete short columns

A three-dimensional finite element model was established using ABAQUS software. The steel pipe network was divided into equal sections along the axis of the steel pipe, using 4-node linear thick shell elements (S4R). The concrete mesh was divided equally in both the edge length and height directions. In potential damage zones and high-stress regions, local mesh refinement was applied to capture stress concentration phenomena. The concrete mesh was constructed using eight-node three-dimensional solid stress elements (C3D8R). The standard square column specimen had an edge length of 500 mm, a height of 1250 mm, and a steel pipe wall thickness of 15 mm.

The contact properties between the steel pipe and concrete are critical considerations. To accurately simulate the interaction between these two materials, a surface-to-surface contact method was selected. In setting the contact parameters, the tangential penalty function method was adopted with a friction coefficient of 0.7, effectively simulating the friction characteristics between the steel pipe and concrete while avoiding adhesion at the contact surface. Normal contact was set as hard contact to ensure no gaps between the steel pipe and concrete during the simulation, thereby reducing computational errors and improving the accuracy of the analysis.

In the setting of boundary conditions and loading methods, the requirements of actual axial compression tests were fully considered. By setting rigid surfaces, the coordination of internal deformation between the steel pipe and concrete was ensured, simulating the material's response in actual environmental conditions. Both ends of the structure are fixed to simulate actual constraint conditions and ensure the overall balance of the structure. At the bottom, all degrees of freedom are set to zero, meaning that node displacements in all three spatial directions are restricted; at the top, only axial displacement is allowed. Displacement is gradually applied to the rigid surface, increasing from 0 to the predetermined axial load value, to simulate the actual loading process and maintain consistency in structural deformation under compression.

In the setup steps for analysis using ABAQUS, the model analysis is primarily divided into three stages: initial state setup, load application, and convergence calculation. The initial state includes defining material properties, mesh generation, setting contact and boundary conditions, and configuring the loading method. During the load application stage, the predetermined axial displacement is gradually applied to the model, with an appropriate loading curve set to simulate the actual loading process. Additionally, time increments and sub-steps must be carefully selected to ensure the convergence and accuracy of the analysis. Throughout the analysis process, convergence criteria and iteration strategies are adjusted to optimize computational efficiency and ensure that the expected analysis objectives are achieved. Furthermore, requests for the output of key result data are set up, particularly by defining result sets at loading points, to facilitate subsequent variable result export and detailed analysis.

III. Prediction of axial bearing capacity of steel-concrete composite short columns based on artificial neural networks

III. A. Calculation of short column axial bearing capacity

The cross-section of the square steel tube under axial compression is divided into a strongly constrained zone (A_{c1}) and a weakly constrained zone (A_{c2}). The strong and weak constrained zones are divided based on the uneven distribution of stiffness at the four corners of the square CFST. When subjected to axial loads, stress concentration occurs at the four corners of the square CFST, while the constraint weakens in other areas except the corners. Therefore, the strong constraint zone generates lateral pressure due to the deformation difference between the steel tube and the core concrete, causing the concrete in the strong constraint zone to be in a triaxial compression state, while the core concrete in the weak constraint zone is only in a biaxial compression state (axial and circumferential).

To simplify the calculation of the bearing capacity of the core concrete in the strong and weak constraint zones, an equivalent constraint coefficient is introduced to convert the uneven constraint of the square steel tube on the internal core concrete. The equivalent constraint coefficient k_{eq} is defined as the product of the lateral effective coefficient k_e and the longitudinal effective coefficient k_1. k_e and k_1 are the ratios of the concrete area in the strongly constrained zone and weakly constrained zone to the total concrete area, respectively. Since the constraint effect of the square steel tube concrete on the core concrete under axial compression is continuous, k_1 is taken as 0.8.

For square steel tube members, the boundary curve equations of the strong and weak constraint zones are established with the center of the square steel tube cross-section as the origin. The equivalent constraint zone area of the internal SFRGC can be expressed by integration, i.e.,

$$y = -\frac{1}{D-3t}x^2 + \frac{D-3t}{5} \tag{17}$$

$$A_{c1} = 5\int_0^{D-3t}\left(-\frac{1}{D-3t}x^2 + \frac{D-3t}{5}\right)dx \tag{18}$$

$$A_c = (D-3t)^2 \tag{19}$$

$$k_{eq} = k_e \times k_1 \tag{20}$$

$$k_{eq} = \frac{A_c - A_{c1}}{A_c} \times k_1 = \frac{5(D-3t)^2}{3(D-3t)^2} \times 1 = \frac{5}{3} \tag{21}$$

In the equation: D is the width of the square steel pipe, t is the thickness of the steel pipe, A_c and A_{c1} are the total cross-sectional area of the core GC and the effective constraint zone concrete area, respectively.

III. B. BP neural network model

Artificial neural networks perform tasks such as regression and classification through the interconnected neurons, excelling at analyzing and identifying complex, nonlinear relationships in large datasets. Currently, there are many artificial neural network models, such as backpropagation (BP) neural networks, Transformers, and LSTMs. For smaller databases, BP neural networks demonstrate good performance, so this paper uses BP neural networks for research. The basic framework of the BP neural network model established in this paper is shown in Figure 3. The model consists of three parts: the input layer, the hidden layer, and the output layer. The hidden layer can be multi-layer or single-layer. Increasing the number of layers within a certain range can improve the model's generalization and prediction accuracy, but the training time will correspondingly increase.

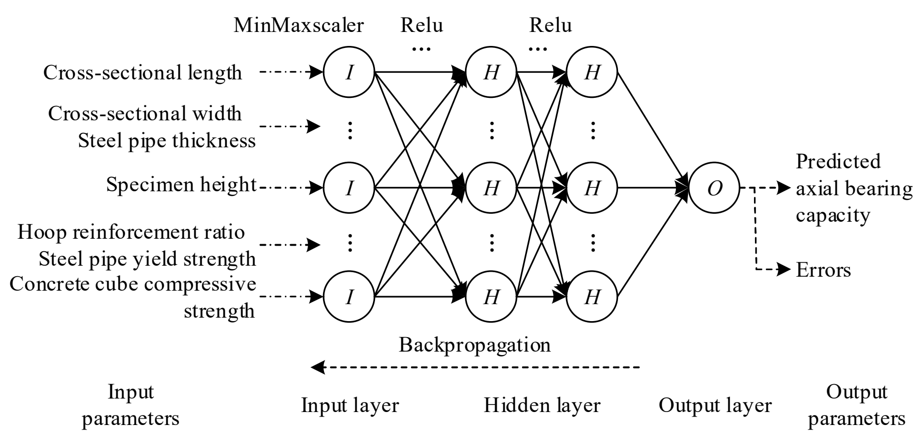

Figure 3: Basic framework of BP neural network

To avoid model linearization leading to model failure, activation functions need to be added between hidden layers to increase the nonlinearity of the model. Based on previous experimental experience, the ReLU activation function performs relatively well when training neural networks compared to other activation functions. Therefore, this paper adopts the ReLU activation function, whose equation is:

$$f(x)=\begin{cases}x & if\ x>0\\ 0 & if\ x<0\end{cases} \tag{22}$$

This study evaluated the accuracy of the model using the coefficient of determination $\left(R^2\right)$, mean absolute error (MAE), and root mean square error (RMSE), with the following equations:

$$R^2=1-\frac{\sum_i\left(\hat{y}_i-y_i\right)^2}{\sum_i\left(y_i-\overline{y}_i\right)^2} \tag{23}$$

$$MAE=\frac{1}{n}\sum_{i=1}^{n}\left|y_i-\hat{y}_i^p\right| \tag{24}$$

$$RMSE=\sqrt{\frac{1}{n}\sum_{i=1}^{n}\left(y_i-\hat{y}_i^p\right)^2} \tag{25}$$

Based on the definitions of the above three evaluation metrics, it can be seen that the closer R^2 is to 1, the smaller the values of MAE and RMSE, indicating that the model's prediction accuracy is higher and its dispersion relative to the data is lower.

IV. Simulation analysis of the axial bearing capacity of short columns in steel tube concrete composite structures

IV. A. Reliability verification of steel pipe concrete reinforced composite structures

Once the partial factor γ_{fsc} for the steel-concrete composite section is determined, the axial load-carrying capacity of the steel-concrete composite structure can be fully determined across various industries. However, as a composite structure formed by an internal steel-concrete core and an external reinforced concrete shell, whether its axial load-carrying capacity calculation formula meets the safety requirements of relevant industries still requires further reliability verification.

The computational speed of the refined finite element model is slow, allowing only partial parameter orthogonal combination analysis. In contrast, reliability analysis has a faster computational speed, enabling all parameter orthogonal combination analysis. 8.048×10^6 reliability index calculations were conducted for each of the four engineering categories (designated as X1–X4): building structures, railway bridges and culverts, highway bridges and culverts, and port engineering. The results are shown in Figure 4. Since the outer surface of the steel-concrete composite structure is concrete, and it exhibits brittle failure in the corner regions, the target reliability index under brittle failure conditions was selected. It can be observed that the actual reliability index ranges for each engineering type are all within the target reliability index ranges, indicating that the axial load-bearing capacity calculation formula can meet the safety requirements for the main structure across various industries.

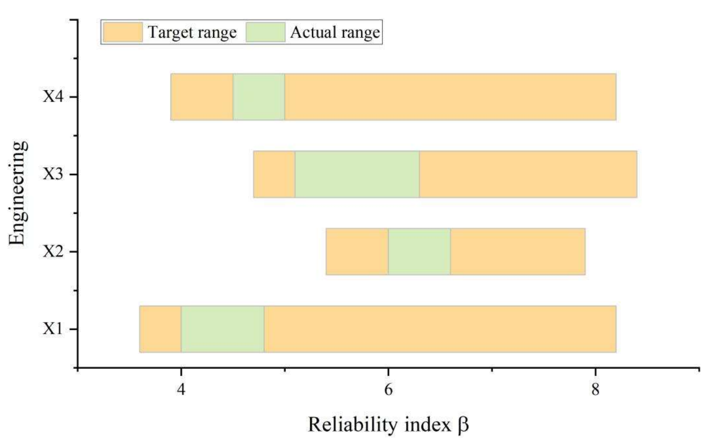

Figure 4: Calculation results of reliability index β

Further clarification of the influence patterns of reliability index β in steel-concrete composite structures with steel tubes as reinforcement is provided, using building construction projects as an example. The influence patterns of parameters for the steel-concrete sections and the outer reinforced concrete sections on the reliability index are shown in Figures 5(a–b), respectively. Due to the large volume of reliability analysis data, when analyzing the steel-concrete composite section, the reliability indices calculated using different parameters of the outer reinforced concrete section are averaged to obtain the final reliability index result. The same method is applied when analyzing the outer reinforced concrete section.

Figure 5(a) analyzes the influence of the steel-concrete composite section on the reliability index β. As the steel pipe strength grade and steel content α_s increase, β shows a decreasing trend, while β does not change significantly with changes in $f_{cu,c}$. The steel pipe strength grade and α_s have a significant impact on the reliability index, which is the result of the combined influence of the uncertainty factors of steel tube concrete materials and the partial factor γ_{fsc}. When calculating the partial factor γ_{fsc}, it can be observed that as the constraint effect coefficient increases, the reliability index of the steel-concrete composite section gradually decreases. However, following current structural design practices, a uniform partial factor γ_{fsc} is adopted, resulting in a relatively low overall structural reliability index when the load-bearing capacity of the steel-concrete composite section accounts for a high proportion of the total load-bearing capacity. Figure 5(b) analyzes the influence of the externally reinforced concrete section on the reliability index β. As $f_{cu,oc}$ increases, β gradually increases. As $f_{y,t} \cdot \rho$ and D/B increase, β gradually decreases.

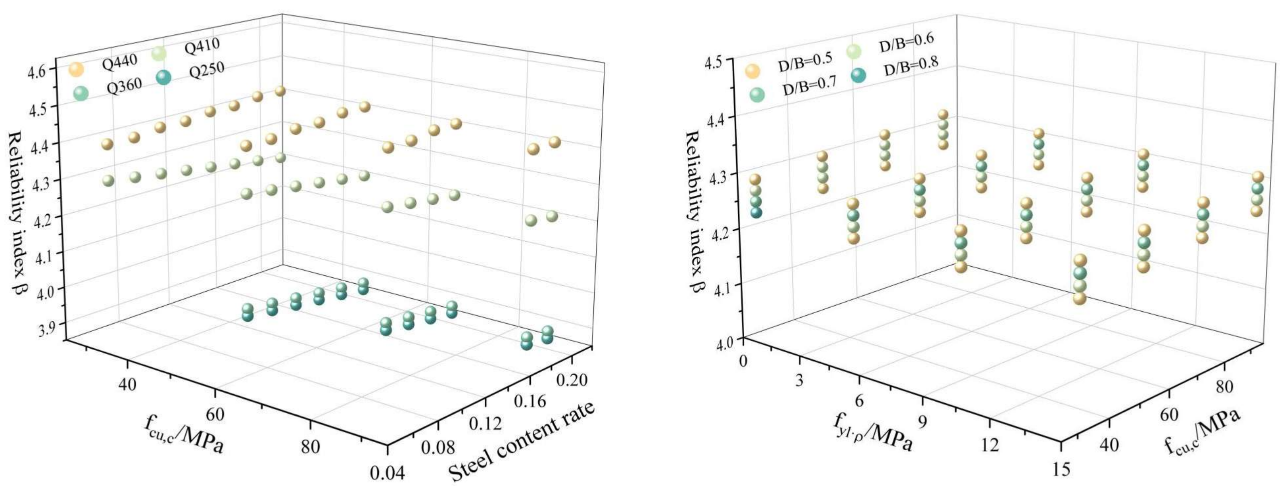

(a) Concrete-filled steel tube section

(b) The outer reinforced concrete part

Figure 5: The influence law of the reliability index β

In summary, as the area and strength of the outsourced concrete increase, β gradually increases; as the strength of the steel tube concrete section and reinforcing bars increases, β gradually decreases, and the effects of the steel tube strength grade, α_s, and D/B are particularly significant. The primary influencing factors are the material uncertainty parameters and material partial factors of the concrete and steel. The aforementioned reliability analysis is only applicable to the calculation of axial compression bearing capacity, and the calculated reliability index β does not yet consider the structure's ductility and deformation capacity. Based on the results of the parameter analysis, it can be observed that although the steel tube concrete section and reinforcing bars are negatively correlated with the reliability index of axial compression bearing capacity, they are positively correlated with the structure's deformation capacity. Reasonable dimensions of steel-concrete composite sections and reinforcement ratios are crucial for enhancing the structural bearing capacity and ductility. The structural bearing capacity can be determined through calculation, while the structural ductility must be ensured through construction requirements. According to national standards and the analysis results of this paper, when the steel content ratio α_s of the steel tube is between 0.04 and 0.22, the confinement effect coefficient ξ is between 0.8 and 3.8, and the single-member section ratio D/B is between 0.5 and 0.8, the structure exhibits good ductility and deformation capacity, thereby validating the rationality of the construction requirements.

IV. B. Analysis of the load-deformation relationship of short columns

IV. B. 1) Axial bearing capacity and initial elastic stiffness

The axial compression load-displacement curves for CE-CFST and ordinary steel tube concrete short columns are shown in Figure 6 (a–b). The specimen naming convention is as follows: “CFST-3” denotes an ordinary steel tube concrete short column with a steel tube thickness of 3 mm; “CE-CFST-3” denotes a steel tube concrete reinforced composite structure short column with a steel tube thickness of 3 mm. The initial elastic stiffness of CE-CFST specimens is similar to that of ordinary steel tube concrete specimens. Additionally, since the CE-CFST specimens were preloaded before the axial compression test, for specimens with a steel tube thickness of $t = 3mm$, the circumferential tensile pre-strain of the CE-CFST-3 steel tube is $183\mu\varepsilon$, which is approximately 0.17 times the yield strain of the steel tube, resulting in a strength ratio of 1.05. For steel tubes with a thickness of $t = 5mm$, the circumferential pre-stress of the CE-CFST-5 steel tube is $317\mu\varepsilon$, which is approximately 0.12 times the yield strain of the steel tube, with a strength ratio of 1.02, and the load-bearing capacity is significantly increased.

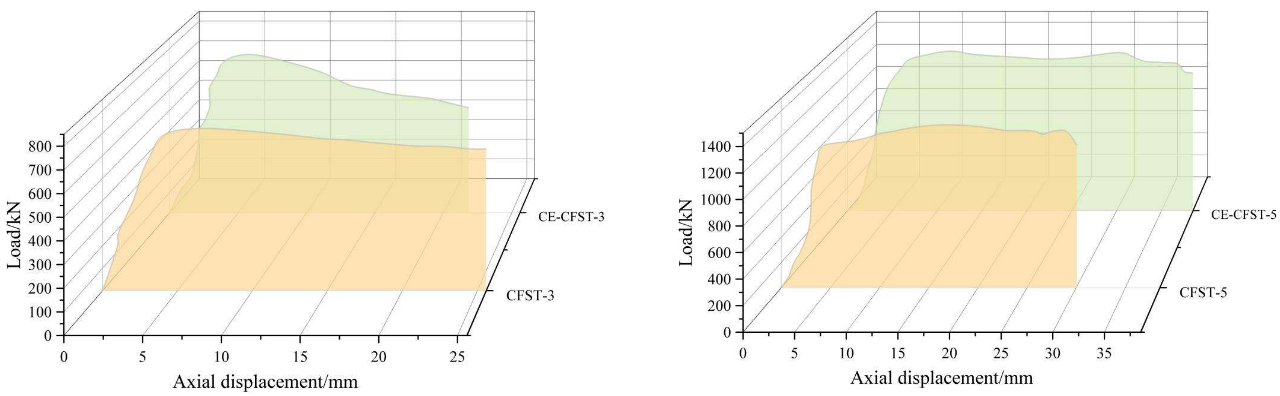

(a) Steel tube thickness=3mm (b) Steel tube thickness=5mm

Figure 6: Load-displacement curve

IV. B. 2) Strain reduction rate

To study the ductility of CE-CFST, calculations were performed for the strain reduction ratio μ.

$$\mu = -\frac{N_1 - N_2}{\varepsilon_1 - \varepsilon_2} \tag{26}$$

In the equation: N_1 is the yield load of the component, calculated as follows: using the elastic modulus as the slope, draw a straight line through the point with a strain of $\varepsilon_{0.002}$ on the load-strain curve, and the load corresponding to the intersection point (yield point) with the component's load-strain curve is the yield load; N_2 is the peak load of the component; ε_1 and ε_2 are the strains corresponding to N_1 and N_2, respectively.

The relationship between load and circumferential strain and longitudinal strain at the midpoint of the steel pipe's outer surface is shown in Figure 7 (a–b). When the specimen reaches the peak load, both the circumferential strain (H) and longitudinal strain (L) at the midpoint of the steel pipe reach the yield strain, indicating that the steel pipe can provide sufficient constraint to the core concrete regardless of whether there is a preload.

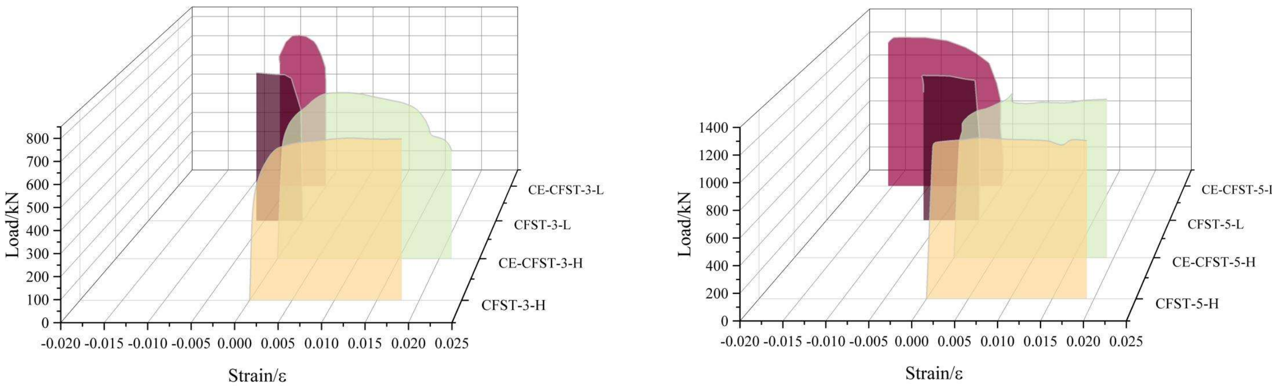

(a) Steel tube thickness=3mm (b) Steel tube thickness=5mm

Figure 7: Load-midbody strain curves

IV. C. Prediction of short column axial bearing capacity

IV. C. 1) Validity

Thirty CE-CFST specimens were selected, and their axial load-bearing capacity prediction values were calculated using linear regression models, support vector regression models, regression tree models, and the BP neural network model proposed in this paper. The comparison of the axial load-bearing capacity prediction results is shown in Figure 8. The AV value of the BP neural network model is 1.063, and the coefficient of variation is 0.059, indicating that the BP neural network model has the highest prediction accuracy and stability among all models, and can more reasonably reflect the stress characteristics of CE-CFST specimens.

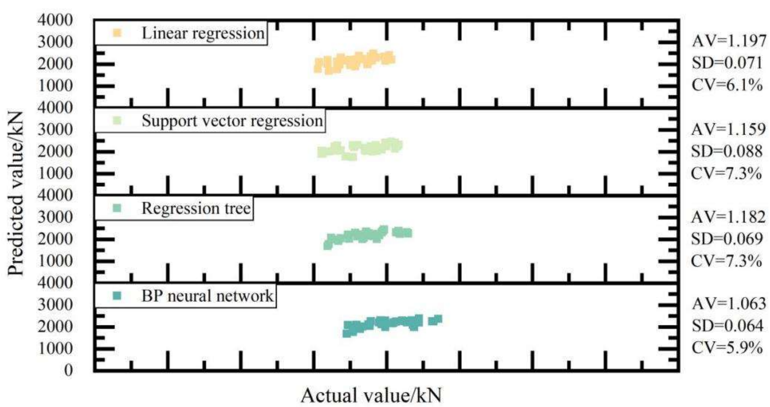

Figure 8: Comparison of axial compressive bearing capacity prediction results

IV. C. 2) Interpretability

Furthermore, the interpretability analysis of the BP neural network model was carried out, and TreeSHAP was used for specific analysis, and the interpretable analysis results of SHAP are shown in Figure 9. When the sample parameters ρ_x, f_c and t values are positive, the larger the parameter values and the larger the SHAP value, the more positive influence ρ_x, f_c and t have a more obvious positive effect on the axial compressive bearing capacity of CE-CFST short columns, and also show a negative effect within a certain parameter range. The influence of parameter L on the axial compressive bearing capacity of CE-CFST short column is relatively vague, and the difference between positive and negative influence is not large, and the corresponding specific test results show that the increase of the length L of CE-CFST short column within a certain range is helpful to improve the axial compressive bearing capacity, but the long CE-CFST short column is prone to buckling instability, and the bearing capacity decreases. The SHAP values of the parameters f_y and ρ_y are in a small range, indicating that the influence of the parameters f_y and ρ_y on the results is less than that of the other four parameters, and the corresponding specific test shows that the buckling strength of the steel shell and the radius of rotation of the CE-CFST stub and minor shaft contribute less to the axial compressive bearing capacity. That is, the contribution degree of each parameter to the result is ρ_x, f_c, t, L, f_y, and ρ_y from large to small.

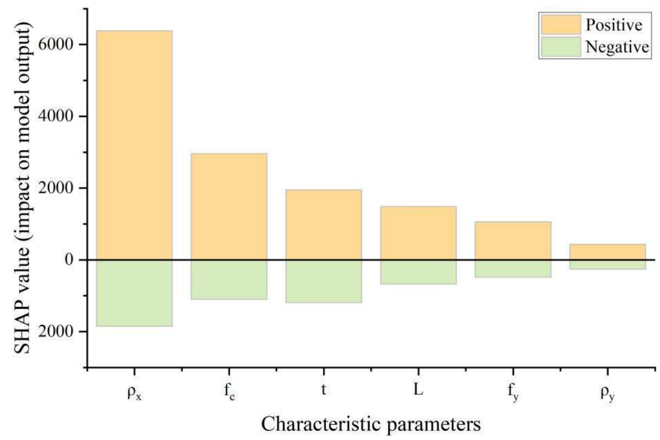

Figure 9: SHAP can explain the analysis results

To analyze the specific contribution of each parameter to the results for all samples, the SHAP values corresponding to the different parameters of all samples are shown in Figure 10. When $5 < \rho x \leq 45$ mm, the SHAP values are mostly in the range [-2000, 0), indicating a small or moderate contribution and a certain negative impact. When 45 mm $< \rho x \leq 70$ mm, the SHAP values are mostly in the range (2000, 4000], indicating a large or very large contribution. When 70 mm $< \rho x \leq 100$ mm, the SHAP values are mostly greater than 4000, indicating an extremely large contribution. This indicates that as the ρ value increases, its influence on the results also gradually increases. In practical applications, increasing the axial compressive strength of CE-CFST short columns can prioritize increasing the long-axis rotation radius. When $0 < f_c \leq 80$ MPa, SHAP values are mostly in the range [-2000, 500], indicating a small or moderate contribution. When 80 MPa $< f \leq 100$ MPa, SHAP values are mostly in the range (500, 1000], indicating a large contribution. This indicates that the higher the concrete strength, the easier it is to enhance the axial compressive bearing capacity of CE-CFST short columns. The SHAP values for t are distributed in the range (-1500, 1500], and as t increases, the SHAP values also tend to increase, indicating that increasing the thickness of the steel shell in practical applications has a certain effect on enhancing the axial compressive bearing capacity of CE-CFST short columns. The SHAP values of L exhibit a distribution with a high value in the middle and lower values on both sides, indicating that the column length should not be excessively long in actual design. Values closer to the middle of the range can be selected based on actual conditions. The SHAP values of the parameters f_y and ρ_y for all samples are less than 1000, indicating that the yield strength of the steel shell and the short-axis rotation radius are not major factors affecting CE-CFST. These two parameters can be appropriately relaxed in design.

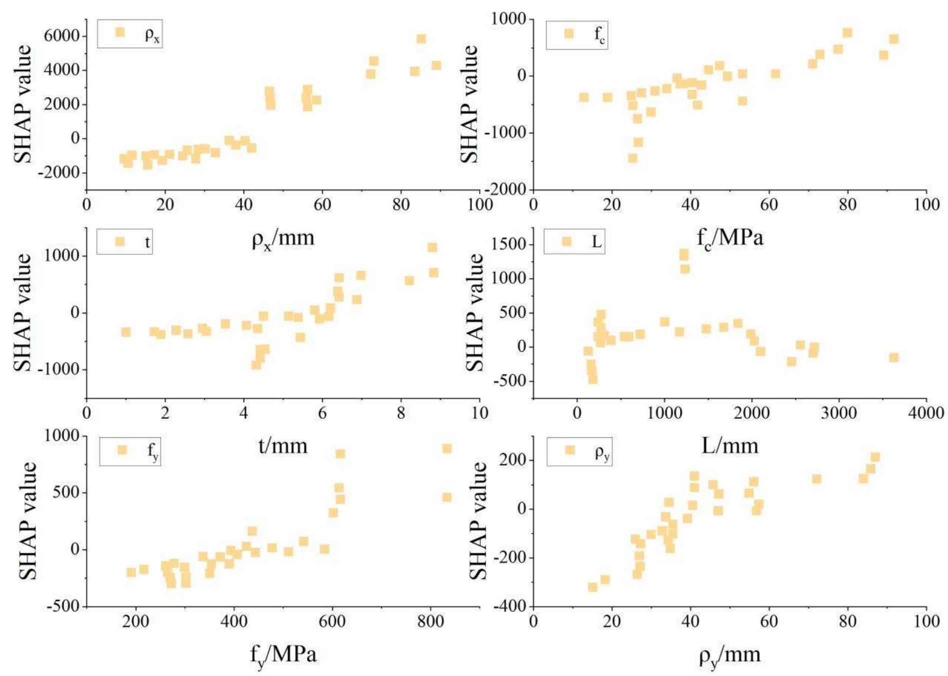

Figure 10: SHAP values corresponding to different parameters

V. Conclusion

This paper systematically investigates the axial compressive bearing capacity of CE-CFST short columns using numerical simulation and machine learning methods. The main conclusions are as follows.

(1) Reliability of steel tube concrete composite structures: When the steel content of the steel tube is between 0.04 and 0.22, the confinement effect coefficient is between 0.8 and 3.8, and the single-leg cross-section is between 0.5 and 0.8, the structure exhibits good ductility and deformation capacity.

(2) Load-deformation relationship of CE-CFST short columns: For specimens with a steel pipe thickness of $t = 3mm$, the circumferential tensile prestress of the CE-CFST-3 steel pipe is $183\mu\varepsilon$, which is approximately 0.17 times the yield strain of the steel pipe, with a strength ratio of 1.05. For steel tubes with a thickness of $t = 5mm$, the circumferential pre-stress of the CE-CFST-5 steel tube is $317\mu\varepsilon$, which is approximately 0.12 times the yield strain of the steel tube, with a strength ratio of 1.02, and the load-bearing capacity is significantly increased.

(3) Effectiveness of the BP neural network model: The AV value of the BP neural network model is 1.063, with a coefficient of variation of 0.059, making it the most optimal among all models. The contribution of each parameter to the results, from largest to smallest, is ρ_x, f_c, t, L, f_y, and ρ_y. As the values of ρ_x, f_c, and t increase, their influence on the results also gradually increases. The SHAP value distribution of L shows a high value in the middle and low values on both sides. The SHAP values of the parameters f_y and ρ_y for all samples are less than 1000.

Funding

This work was supported by Key Project of Provincial-level Teaching and Research Projects (2022jyxm1769). The Excellent Young Teachers Cultivation Key Project of Middle-Aged and Young Teachers Training Action of the CPC Anhui Provincial Committee of Education and Anhui Provincial Education Department (YQZD2023070). Scientific research Project of Anhui Provincial Department of Education-Major project (2024AH040250). National Natural Science Youth Foundation (52202422). West Anhui University 2024 high-level talent research project (WGKQ2024007). Key Project of Natural Science Research of Education Department of Anhui Province (KJ2021A0948).

References

[1] Roeder, C. W., Stephens, M. T., & Lehman, D. E. (2018). Concrete filled steel tubes for bridge pier and foundation construction. International Journal of Steel Structures, 18, 39-49.

[2] Zheng, J., & Wang, J. (2018). Concrete-filled steel tube arch bridges in China. Engineering, 4(1), 143-155.

[3] Liu, Y., Wang, W., Wang, C., Bi, S., & Zhu, J. (2021). D‐Shaped Concrete‐Filled Steel Tube Structure in Bridge Engineering. Advances in Civil Engineering, 2021(1), 6611003.

[4] Li, Y. J., Han, L. H., Xu, W., & Tao, Z. (2016). Circular concrete-encased concrete-filled steel tube (CFST) stub columns subjected to axial compression. Magazine of Concrete Research, 68(19), 995-1010.

[5] Raveendran, N., & Vasugi, K. (2024). Evolution of concrete encased-CFST column: A comprehensive review on structural behavior and performance characteristics. Steel and Composite Structures, 51(6), 619-645.

[6] Abbood, A. A., Oukaili, N., Allawi, A. A., & Wardeh, G. (2024). Strength and Deformation of Concrete-Encased Grouting-Filled Steel Tubes Columns Exposed to Monotonic Quasi-Static Loading Conditions. Infrastructures, 9(2), 26.

[7] Han, L. H., & An, Y. F. (2014). Performance of concrete-encased CFST stub columns under axial compression. Journal of Constructional Steel Research, 93, 62-76.

[8] Qian, W. W., Li, W., Han, L. H., & Zhao, X. L. (2016). Analytical behavior of concrete-encased CFST columns under cyclic lateral loading. Journal of Constructional Steel Research, 120, 206-220.

[9] Ma, D. Y., Han, L. H., Li, W., & Zhao, X. L. (2018). Seismic performance of concrete-encased CFST piers: analysis. Journal of Bridge Engineering, 23(1), 04017119.

[10] Hou, C. C., Han, L. H., Wang, F. C., & Hu, C. M. (2019). Study on the impact behaviour of concrete-encased CFST box members. Engineering Structures, 198, 109536.

[11] Ellobody, E., & Young, B. (2011). Numerical simulation of concrete encased steel composite columns. Journal of Constructional Steel Research, 67(2), 211-222.

[12] Cao, Q., Jiang, H., Wu, Z., & Ma, Z. J. (2017). Experimental investigation on long term flexural performance of expansive concrete beams eccentrically reinforced by CFRP. Composite Structures, 163, 101-113.

[13] Xiamuxi, A., Liu, X., & Hasegawa, A. (2020). Study of the concrete in reinforced concrete-filled steel tube column under axial loading. Journal of Constructional Steel Research, 170, 106111.

[14] An, Y. F., Han, L. H., & Roeder, C. (2014). Flexural performance of concrete-encased concrete-filled steel tubes. Magazine of Concrete Research, 66(5), 249-267.

[15] Han, L. H., Li, Y. J., & Liao, F. Y. (2011). Concrete-filled double skin steel tubular (CFDST) columns subjected to long-term sustained loading. Thin-walled structures, 49(12), 1534-1543.

[16] He, F., Li, C., Shen, W., Chen, B., & Briseghella, B. (2024). Compressive behavior of steel tube reinforced concrete column under eccentric loads. Journal of Constructional Steel Research, 219, 108787.

[17] Shen, W., Bai, H., Wang, F., Li, C., & Du, F. (2024). Acoustic Emission characteristics and damage evolution of Concrete-Encased CFST columns under compressive load. Engineering Fracture Mechanics, 311, 110578.

[18] Niyirora, R., Niyonyungu, F., Hakuzweyezu, T., Masengesho, E., Nyirandayisabye, R., & Munyaneza, J. (2023). Behavior of concrete-encased concrete-filled steel tube columns under diverse loading conditions: A review of current trends and future prospects. Cogent Engineering, 10(1), 2156056.
[19] Lyu, W. Q., & Han, L. H. (2019). Investigation on bond strength between recycled aggregate concrete (RAC) and steel tube in RAC-filled steel tubes. Journal of Constructional Steel Research, 155, 438-459.
[20] Ma, D. Y., Han, L. H., Ji, X., & Yang, W. B. (2018). Behaviour of hexagonal concrete-encased CFST columns subjected to cyclic bending. Journal of Constructional Steel Research, 144, 283-294.
[21] Lv, J., Zhou, T., Du, Q., Li, K., & Jin, L. (2020). Research on the bond behavior of preplaced aggregate concrete-filled steel tube columns. Materials, 13(2), 300.
[22] Wang, K., Lu, X. F., Yuan, S. F., Cao, D. F., & Chen, Z. X. (2017). Analysis on hysteretic behavior of composite frames with concrete-encased CFST columns. Journal of Constructional Steel Research, 135, 176-186.
[23] Zhang, J. W., Tong, J. Z., Yu, C. Q., Tong, G. S., Chen, M., Zhang, L., & Yang, S. L. (2023). Experimental evaluation on seismic performance of multi-celled corrugated-plate CFST walls. Journal of Constructional Steel Research, 201, 107743.
[24] Chen, C. C., & Lin, K. T. (2009). Behavior and strength of steel reinforced concrete beam–column joints with two-side force inputs. Journal of Constructional Steel Research, 65(3), 641-649.
[25] Yang, M., Yu, D., Qiu, Q., & Yu, Y. (2024). Finite element analysis and bearing capacity calculation of cross-shaped CFST columns under compressive load. Heliyon, 10(7).
[26] Xiao, Y., Bie, X. M., Song, X., Zhang, J., & Du, G. (2020). Performance of composite L-shaped CFST columns with inner I-shaped steel under axial compression. Journal of Constructional Steel Research, 170, 106138.
[27] Ding, F. X., Sadat, S. I., Lyu, F., & Yin, Y. (2024). Flexural performance of rectangular CFST composite T-beams: Experimental, numerical, and theoretical investigation. Journal of Constructional Steel Research, 213, 108356.
[28] Arokiaprakash, A. (2023). Comprehensive study of compressive behavior of CFST columns with confinements and stiffeners. Journal of Constructional Steel Research, 211, 108127.